Journal of Solid State Chemistry **150,** 196–203 (2000)
doi:10.1006/jssc.1999.8583, available online at http://www.idealibrary.com on IDEAL®

Effects of Partial Acid Delithiation on the Electrochemical Lithium Insertion Properties of Nickel-Stabilized $LiMn_2O_4$ Spinel Oxides

P. Lavela, L. Sánchez, and J. L. Tirado[1]

Laboratorio de Química Inorgánica, Facultad de Ciencias, Universidad de Córdoba, Avenida San Alberto Magno s/n, 14004 Córdoba, Spain

and

S. Bach and J. P. Pereira-Ramos

Laboratoire d'Electrochimie, Catalyse et Synthèse Organique, LECSO-CNRS UMR 7582, 2 rue Henri Dunant, 94320 Thiais, France

Received July 14, 1999; in revised form November 5, 1999; accepted November 22, 1999

Use of nickel-containing $LiMn_2O_4$ up to 20 at.% as an insertion electrode in lithium cells combined with preliminary acid treatment results in improved cycling performance. An increase in the average oxidation state of manganese, a decrease in the Li/Mn ratio, partial H^+/Li^+ exchange, and a decrease in the unit cell parameters of the solid products take place during treatment with aqueous HNO_3. X-Ray diffraction line broadening analysis shows that for a sample with a Ni/Mn ratio of 0.25 and a temperature of preparation of 800°C, crystallinity increases slightly with acid treatment, as a result of the dissolution of the external layers of the solid in which defects concentrate. For samples prepared below 800°C an increase in line broadening associated with a larger extension of the cation-exchange process is observed. The use of acid-treated solids in lithium cells results in higher capacities and better capacity retention as compared with pristine spinels. Larger capacities are always observed for samples prepared at 550°C and a Ni/Mn ratio of 0.11. The role of nickel is of particular interest in stabilizing the spinel structure and allowing high average oxidation states of manganese in the solid.

INTRODUCTION

The attracting electrochemical properties of spinel phases in the Li–Mn–O system have been extensively studied since the early reports by Thackeray *et al.* (1, 2). The studies on $LiMn_2O_4$ were reinforced by their implementation in Li ion cells by Tarascon and Guyomard (3) Nevertheless, the favorable properties of these electrodes—high potential versus lithium, low toxicity, and low molecular weight—are shadowed by undesirable capacity fading phenomena, particularly marked on prolonged cycling in the 3-V region at room temperature or in the 4-V region at 55°C and higher (4). Different attempts to avoid the negative effects include partial substitution of manganese with other elements such as Ni, Co, and Cr (5, 6). Among the nickel-substituted $LiMn_2O_4$ several examples of good capacity retention behavior have been reported (7–9). Alternatively, the use of other lithium manganese (IV)/(III) spinel oxides diverging from $LiMn_2O_4$ stoichiometry reveals several phases of interest (10). By combining both possibilities, Co-substituted $Li_2Mn_4O_9$ oxides were recently found to have good capacity retention (11).

On the other hand, cycling performance was found to be improved in layered oxides such as $Li(Co_{1-y}Ni_y)O_2$ by chemical delithiation in acid medium (12, 13). The chemical reaction with hydrochloric acid leads to nickel disproportionation and partial dissolution of the solid, while the remaining oxide contains a larger amount of Ni(IV) and lower lithium content (14). A similar chemical delithiation process was first described by Hunter (15) for $LiMn_2O_4$, leading to the λ-MnO_2 phase by a manganese disproportionation reaction accompanied by Mn^{2+} dissolution. Attempts to use the form dioxide as electrode material by Manev *et al.* (16) showed important difficulties. Recently, Tarascon and co-workers (17) used the chemical deintercalation of $LiMn_2O_4$ as an interesting route to prepare different phases of manganese dioxide in the presence of different species in solution. The presence of bismuth in the reaction medium was found to limit spinel oxide dissolution and to affect the kinetics of the λ to α/γ-MnO_2 transformation.

More recently, Feng *et al.* (18–20) observed that lithium extraction from nonstoichiometric lithium manganese oxide $Li_{1.33}Mn_{1.67}O_4$ (18) and $LiM_xMn_{2-x}O_4$ with $M = Mg$ (19) and Zn (20) ($x = 0.5$) is accompanied by a partial H^+/Li ion-exchange process and fractional extraction of M. The

[1]To whom correspondence should be addressed. Fax: 34 957 218606. E-mail: iq1ticoj@lucano.uco.es.

0022-4596/00 $35.00

interpretation given to these observations is based on the assumption that the numbers of redox-type and ion-exchange-type sites correlate well with the amounts of trivalent Mn ions and Mn defects, respectively (18).

The aim of this work is to show the advantages of combining nickel substitution with partial chemical delithiation in $LiMn_2O_4$. A synthetic route based on the coprecipitation of mixed Mn–Ni carbonate precursors is used in the preparation that allows a uniform cation distribution of both transition metal elements in the octahedral sites of the lithium-containing spinel oxide. Optimization of nickel content, thermal treatment, and acid treatment conditions leading to better yield and performance is also discussed.

EXPERIMENTAL

Three sets of metal-substituted spinel oxides of general formula $Li(Mn_{1-y}Ni_y)_2O_4$ ($y = 0.05, 0.1, 0.2$) were prepared from intimately ground mixtures of Li_2CO_3 and mixed carbonates of $(Mn_{1-y}Ni_y)CO_3$ stoichiometry. The powder mixtures were heat-treated in an air atmosphere at different temperatures in the range 380–800°C. The carbonate precursors were prepared by the addition of a 1 M solution of $NaHCO_3$ to a 0.5 M solution of the divalent ions Ni^{2+} and Mn^{2+} under continuous flow of CO_2. Chemical deintercalation was carried out by acid treatment of the metal-substituted spinel oxides. Aqueous HNO_3 solutions with 0.1 and 1.0 M concentrations and reaction periods of 48 and 24 h, respectively, were used to compare the chemical and electrochemical results.

Li/Mn and Ni/Mn ratios were determined by atomic absorption measurements after complete dissolution of the pristine and acid-treated solids. The average oxidation state of metal ions in the solid samples was determined by the following procedure. About 20 mg of sample was dissolved in 25 ml of 0.1 M Fe^{2+} in 0.01 M H_2SO_4 under continuous flow of argon and heated until complete dissolution. The solution was titrated with standard 0.001 M $KMnO_4$. Previously the $KMnO_4$ solution was normalized with $Na_2C_2O_4$. The titrations were assigned to the excess of Fe^{2+} ions in the sample and were used to calculate the average oxidation state of manganese (Mn O.S). The stoichiometry was confirmed by energy-dispersive X-ray microanalysis coupled to a *JEOL* JSM6300 scanning electron microscope. The XRD data were collected with a *Siemens* D-5000 X-ray diffractometer using Cu$K\alpha$ radiation and a graphite monochromator. Step-scan recordings were carried out for the Rietveld structural analysis by using 0.04°2θ steps of 6-s duration. The computer program DBWS9000 was used in the calculations (21). Thermogravimetric (TG) and differential thermal analysis (DTA) curves were obtained by using a Setaram Model SETSYS-12 apparatus. FTIR spectra were obtained with a Bomem apparatus.

Electrochemical studies were carried out in two-electrode cells. The electrolyte used was 1 M $LiClO_4$, previously dried under vacuum at 170°C for 16 h, in distilled ethylene:propylene carbonate (1:1 mixture). The oxide electrode pellets (7 mm in diameter) were prepared by pressing at 4 tons ca. 3 mg of active material with PTFE (5 wt%), graphite (7.5 wt%), and acetylene black (7.5 wt%) on a steel grid. Lithium foil was cut as 7-mm-diameter circles and was used as the anode versus the spinel oxide electrode. Unless otherwise specified, the cells were cycled at 0.25 mA/cm^2 current densities, which were controlled with a MacPile II potentiostat–galvanostat (22). Step potential electrochemical spectroscopy (SPES) spectra were recorded under different kinetic conditions.

RESULTS AND DISCUSSION

Three nickel-containing $LiMn_2O_4$-related samples of different compositions were prepared by varying the nickel content in the precursor and the temperature of thermal treatment. The solids are henceforth referred to as samples (A) $Li(Ni_{0.05}Mn_{0.95})_2O_4$, prepared at 380°C, (B) $Li(Ni_{0.1}Mn_{0.9})_2O_4$ (550°C), and (C) $Li(Ni_{0.2}Mn_{0.8})_2O_4$ (800°C), obtained by chemical analysis of the oxide products (see Table 1). From the chemical titration of the average

TABLE 1
XRD and Chemical Parameters of Pristine and Acid-Treated Samples

Sample	a (Å)	FWHM (1 1 1)°2θ	Oxidation state of Mn	H/Mn	Li/Mn	Ni/Mn	Formula
A	8.133(4)	0.652	3.57	0.00	0.53	0.05	$LiNi_{0.1}Mn_{1.9}O_4$
B	8.146(1)	0.453	3.67	0.00	0.56	0.11	$LiNi_{0.2}Mn_{1.8}O_4$
C	8.1804(3)	0.145	3.88	0.00	0.63	0.25	$LiNi_{0.4}Mn_{1.6}O_4$
A1	8.11(1)	0.849	3.77	0.80	0.26	0.05	$Li_{0.42}H_{1.30}Ni_{0.08}Mn_{1.63}O_4$
B1	8.124(5)	0.492	3.93	0.36	0.36	0.11	$Li_{0.60}H_{0.60}Ni_{0.18}Mn_{1.65}O_4$
C1	8.1434(2)	0.124	3.97	0.17	0.52	0.25	$Li_{0.81}H_{0.26}Ni_{0.39}Mn_{1.55}O_4$
A2	8.093(6)	1.022	3.75	0.77	0.24	0.05	$Li_{0.39}H_{1.26}Ni_{0.08}Mn_{1.64}O_4$
B2	8.125(6)	0.499	3.92	0.13	0.37	0.11	$Li_{0.64}H_{0.22}Ni_{0.19}Mn_{1.72}O_4$
C2	8.1355(3)	0.122	4.00	0.20	0.53	0.25	$Li_{0.81}H_{0.30}Ni_{0.38}Mn_{1.53}O_4$

oxidation state of metal ions in the samples, the composition always agreed with an O/M ratio close to 2. On the assumption of Ni being in the 2+ oxidation state, as suggested by Zhong *et al.* (7) from the constancy in the electrochemical capacity of similar solid solutions in both the 4.1- and 4.7-V plateaus, the compositions imply that the average oxidation state of manganese increases with nickel content, being 3.57, 3.67, and 3.88 for samples A, B, and C, respectively.

The X-ray diffraction patterns of the three pristine samples (Fig. 1) could be indexed in the cubic spinel structure of $LiMn_2O_4$ (23). The effect of thermal treatment was evidenced by the enhanced line broadening observed in the lower-temperature samples, as a result of the increase in crystallinity on increasing preparation temperature. Due to the enhanced broadening of the line profiles, a complete Rietveld refinement of the structural parameters was not fully successful in samples prepared below 800°C. Nevertheless, the separate refinement of the cubic unit cell parameter

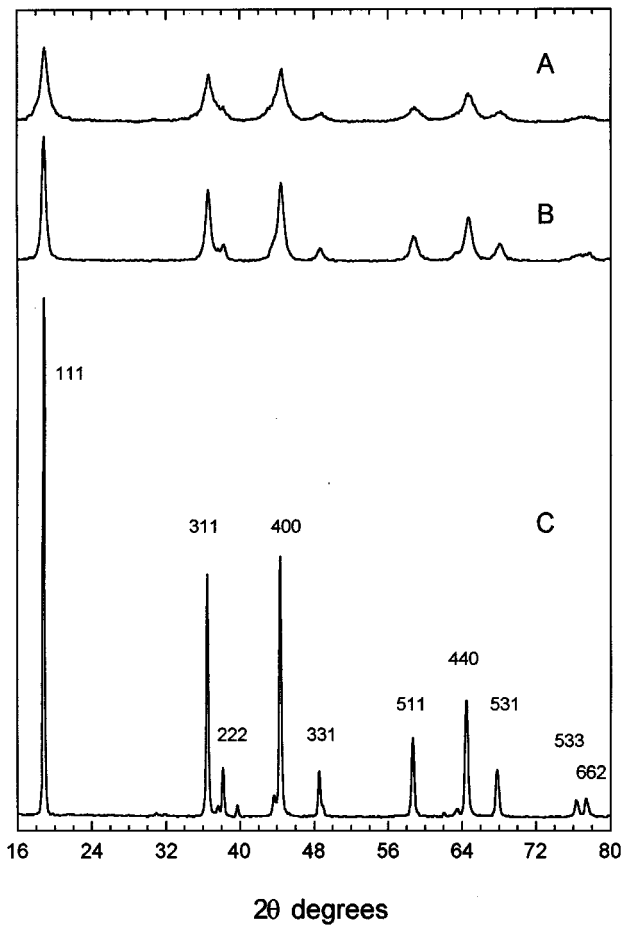

FIG. 1. X-ray powder diffraction patterns of samples (A) $Li(Ni_{0.05}Mn_{0.95})_2O_4$, obtained at 380°C; (B) $Li(Ni_{0.1}Mn_{0.9})_2O_4$, obtained at 550°C; and (C) $Li(Ni_{0.2}Mn_{0.8})_2O_4$, obtained at 800°C.

a allowed us to observe lower values than in $LiMn_2O_4$, (Table 1) which agrees with previous reports (7). For sample C, $Li(Ni_{0.2}Mn_{0.8})_2O_4$, the refinement of XRD patterns could be carried out by using the Rietveld method. The best fit was obtained by using the $Fd\bar{3}m$ space group of the cubic spinel and assuming a statistical distribution of nickel and manganese atoms in the 16*d* sites. The following parameters were then obtained: $R_{BRAGG} = 3.99$, $S(R_{wp}/R_{expected}) = 0.41$, and z_{oxygen} (32*e* sites) = 0.2607(5). The amount of lithium was also refined and agreed well with the chemical analysis.

Acid treating the nickel-containing spinel compounds resulted in a solid product in which the average oxidation state of manganese increased and the Li/Mn ratio decreased, while the Ni/Mn ratio remained basically unaffected (Table 1). From these results, it can be seen that the changes in Mn/Li ratio are only slightly affected by the two different acid treatment procedures followed here, which differed in both acid concentration and duration of reaction. In addition, chemical analysis of the nitric acid solutions used in the treatments revealed a significant content of lithium, manganese, and nickel, thus indicating partial dissolution of the solid. In a first approach, these results could be interpreted in agreement with the description given by Hunter (15) to the reaction of $LiMn_2O_4$ in acid medium to give the λ-MnO_2 phase by a manganese disproportionation reaction accompanied by Mn^{2+} dissolution:

$$2LiMn_2O_4 + 2H^+Li_2O + 3MnO_2 + Mn^{2+} + H_2O. \quad [1]$$

It should be noted that if lithium deinsertion was the only process taking place, the minimum Li /Mn ratios that could be allowable by assuming a maximum oxidation state of manganese of 4+ and retaining the 2+ oxidation state of nickel (7) are 0.11, 0.22, and 0.50 for samples An, Bn, and Cn, respectively. The experimental Li/Mn values observed in Table 1 are always above the theoretical values.

However, the possible H^+/Li^+ exchange reaction for the nickel-containing samples similar to those found for $LiFeMnO_4$ (24), $LiMg_{0.5}Mn_{1.5}O_4$ (19), and $LiZn_{0.5}Mn_{1.5}O_4$ (20) should be taken into account. Thus, additional experiments were carried out. FTIR spectra of original and acid-treated samples are shown in Fig. 2. In agreement with the results of Feng *et al.* (18–20, 24), the spectra show the presence of hydrogen in the acid-treated solids. The weak band at ca. 3340 cm^{-1} is ascribable to stretching vibrations of lattice–OH groups. The band at ca. 910 cm^- has been ascribed to lattice coupling vibrations of the H^+-form spinel.

To quantify the amount of hydrogen in the structure of the solids, DTA and TG recordings were obtained (Fig. 3). These data show several endothermal effects below 800°C, accompanied by weight loss processes. The effect at ca. 200°C has been ascribed to the release of water from lattice–OH groups (19, 20). From these results, the evaluation

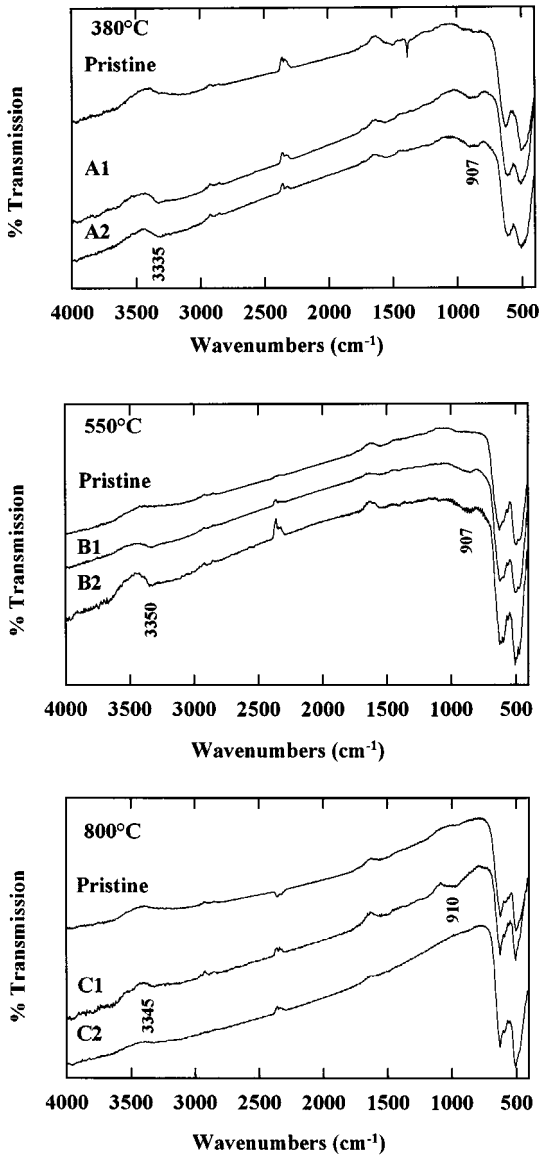

FIG. 2. FTIR spectra of (A–C) pristine samples, (A1–C1) samples treated 48 h with 0.1 M HNO_3, and (A2–C2) samples treated 24 h with 1.0 M HNO_3.

of hydrogen content in the samples was carried out from the weight loss in the interval 120–300°C. These data are also included in Table 1 and were used to calculate the complete stoichiometry of the products, as derived from the electroneutrality principle. It can be seen that the level of cation exchange increases as synthesis temperature and crystallinity decrease. From Fig. 3, it is also evident that the composition of the products leads to stoichiometric numbers of hydrogen which are higher than those expected from a simple Li/H exchange. Feng *et al.* (19, 20) also found an excess of protons with respect to the initial lithium content which was unambiguously ascribed to the exchange of some metal cations different from lithium by protons during acid treatment of Zn- and Mg-containing spinels. In our case this possibility seems obvious as the O/(Mn + Ni) ratio increases with acid treatment. The loss of nickel and manganese accounts for the excess of protons.

Nevertheless, the presence of a true disproportion/partial dissolution process cannot be discarded, as found by the net increase in the average oxidation state of manganese and by analysis of the acid solution used in the treatment. Again, the dependence on temperature is clear and opposite to the extent of H^+/Li^+ exchange: as crystallinity decreases the final average oxidation state of manganese in the acid-treated samples is lower.

The effects of these reactions were also patent in the X-ray diffraction patterns of the solid products treated with aqueous HNO_3. The cubic unit cell parameter *a* (Table 1) decreased significantly with lithium extraction, as found in previous work (15). Again, the differences between treatments 1 and 2 are not marked. Due to the presence of the lighter element hydrogen, a complete Rietveld analysis of the acid-treated samples had to be discarded. Table 1 also includes the experimental full width at half-maximum (FWHM) values of the (111) profiles of all samples. It can be seen that a slight but significant decrease in linewidth with acid treatment is observed for sample C. However, for samples A and B, a marked increase in FWHM is observed with acid treatment. The differences can be related to the different extension of the H^+/Li^+ exchange process for each

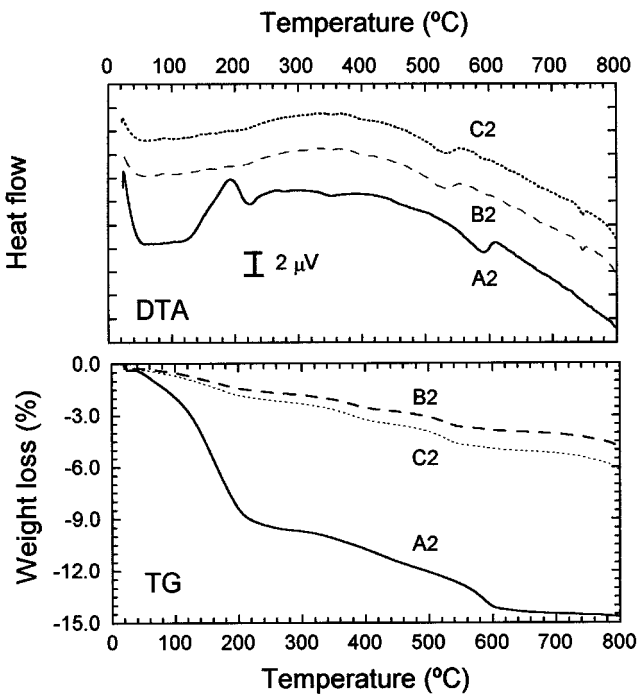

FIG. 3. TG and DTA curves of selected acid-treated samples.

sample. Thus, low-temperature samples show marked extension of the exchange process and a less marked manganese oxidation which may result in important lattice distortions. On the contrary, for sample C the dissolution process prevails but affects only the external layers of the particles, where the defects may concentrate.

To evaluate the effect of acid treatment on the lithium extraction–insertion properties of the nickel-containing spinels, SPES experiments of lithium cells were carried out using the different samples as active cathode material. Figures 4 and 5 contain the complete curves for samples C, C1, and C2. For all samples, the as-prepared cells built up with the chemically deintercalated cathodes showed higher values of near to open circuit voltage, as referred to the pristine cathodes. The chemical extraction of lithium from tetrahedral sites and the simultaneous increase in the manganese oxidation state increase significantly the free energy of these materials. For C samples, this fact is supported by the occurrence of a initial smooth voltage drop that can be ascribed to the lithium insertion in these new chemically created sites (Fig. 4). Moreover, the Faradaic yield at the end of this region of the first discharge curve in acid-treated samples was used to obtain an alternative evaluation of the extension of the lithium extraction process. The values obtained by this parallel procedure agree fairly well with those obtained by the change in oxidation state of manganese derived by chemical analysis. On the contrary, in the potentiostatic discharges of chemically deintercalated spinels obtained below 800°C (samples A and B), although an increase in the initial voltage is observed, the subsequent discharge does not show the presence of any quasi-plateau at higher voltages. This phenomenon is probably due to the lower crystallinity of these samples which creates new tetrahedral sites but with diverging free energies.

The initial increase in cell capacity with cycle number observed for sample C in Fig. 4 may be ascribed to flexibilization of the lattice after the electrochemical lithium extraction. This phenomenon is not needed in acid-treated samples, as partial extraction is carried out by the prior chemical treatment. The extended charge plateaus in cycle 5 for the acid-treated sample C1 imply solvent decomposition due to the high voltage reached. This was avoided by choosing a narrower potential window (2.5–3.5 V) in the cycling experiments discussed below.

Figure 5 shows the voltammograms of charge and discharge for sample C treated with 0.1 and 1.0 M HNO_3 for 48 and 24 h, respectively. The SPES methodology is a powerful tool to discern between small structural transitions during lithium insertion/deinsertion. The intensity-versus-voltage curves show the coexistence of pseudophases as clearly resolved bands. The main reduction and oxidation peaks for the first cycle appear slightly polarized with respect to these of pristine sample. Nevertheless, the behavior through several cycles makes it evident that these peaks are displaced

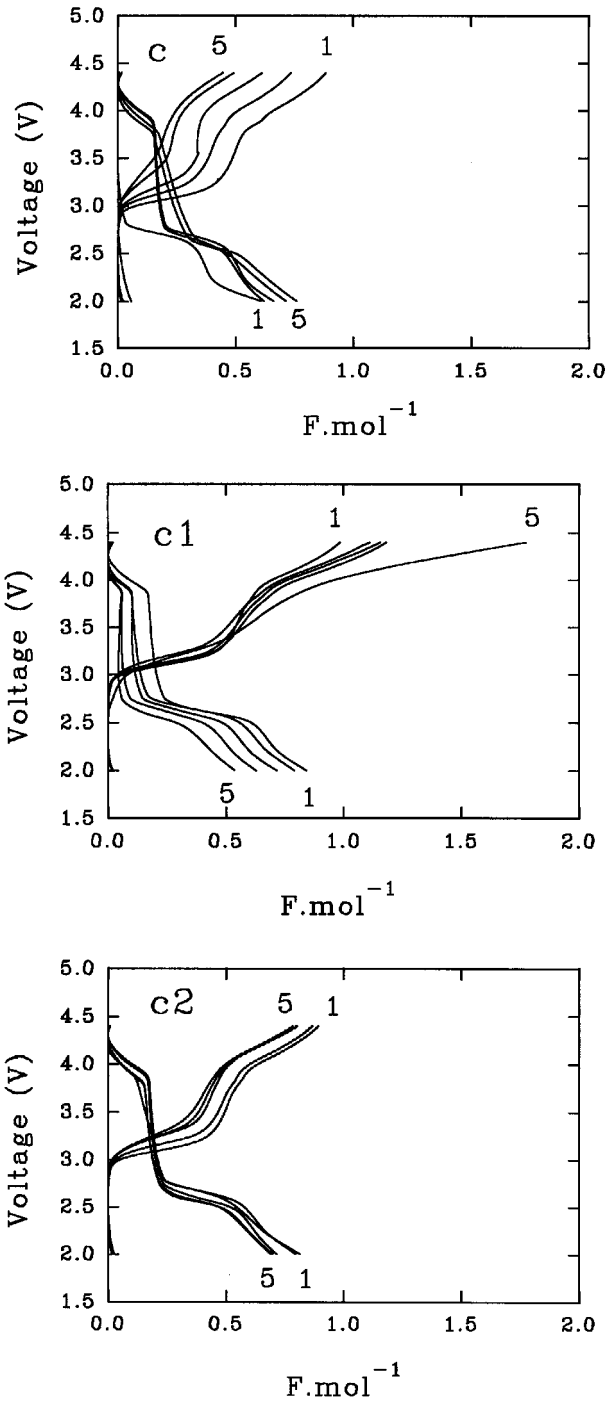

FIG. 4. Cell voltage (V) versus composition (F/mol) curves obtained by step potential electrochemical spectroscopy of lithium cells using samples C, C1, and C2 as active cathode materials.

toward lower values in reduction and higher values for oxidation accompanied by a broadening. The shape of the reduction curves evidences a more rapid transition of the cell potential in pristine compounds, while for acid-treated

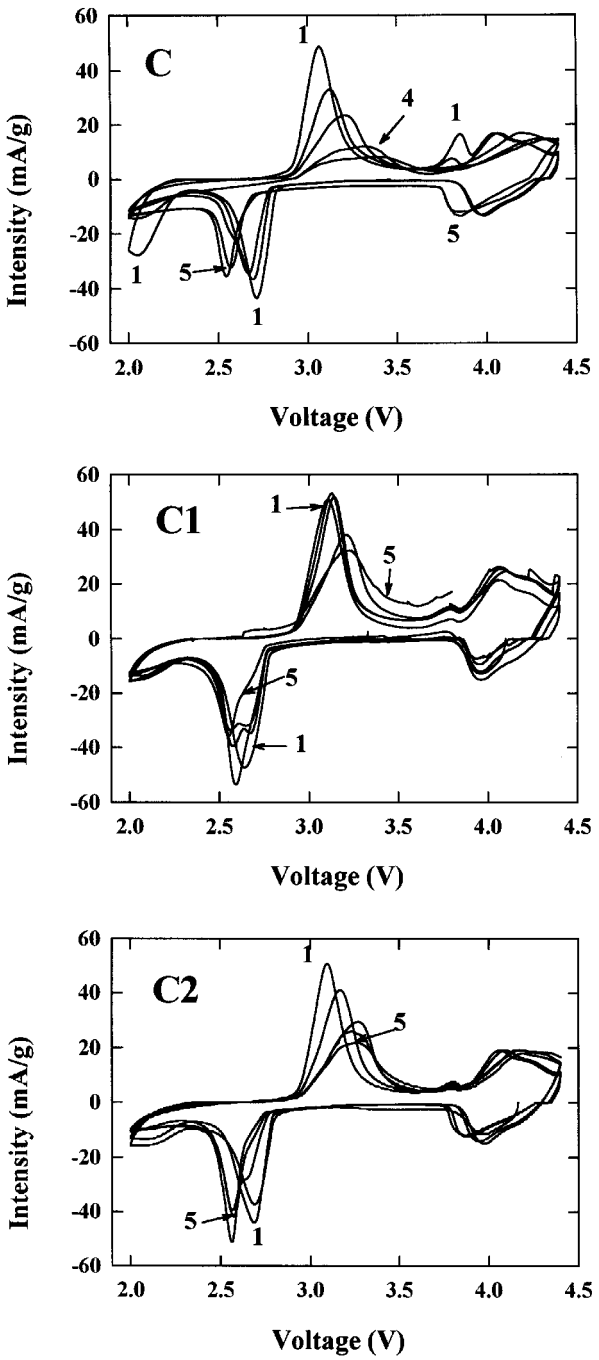

FIG. 5. *i–V* curves obtained by step potential electrochemical spectroscopy of lithium cells using samples C, C1, and C2 as active cathode materials.

samples a splitting of the main signals is observed. In the same sense, oxidation curves show a higher polarization and broadening of the main signal for pristine than for deintercalated compounds. These results imply that chemically deintercalated samples suffer smaller structural changes that affect the alkaline ion pathways through the spinel structure. Two main consequences can be extracted from these results: (a) the initial diffusion is hindered; (b) this negative effect is overcome in part for further cycles, possibly due to an increase in the adaptability of the deinserted network to a continuous process of charge and discharge.

On the contrary, the acid treatment with a highly concentrated solution of 1 M HNO_3 was less favorable, as reflected in the location of the reduction and oxidation bands, which is more similar to that of the pristine spinel. Probably, the higher concentration of acid provokes a more extended occurrence of partial dissolution reaction that distorts the host network.

The structural changes induced during the first discharge–charge cycle on the solids were followed by X-ray diffraction of the electrodes obtained by interrupting the discharge experiments at different depths. An enhanced line broadening of the (400) and (440) lines was observed in the electrochemically intercalated samples [see Fig. 6 for (400) profiles of sample B after acid treatment with 0.1 M HNO_3 for 48 h]. This effect can be ascribed to the coexistence of the cubic spinel solid and a tetragonally distorted spinel phase resulting from the Jahn–Teller effect of Mn^{3+} ions (10). Thus, it can be derived that the tetragonal distortion also affects this material for the deeply discharged electrode.

Figure 7 shows the changes in capacity during the first cycles for pristine B (obtained at 550°C) and C (800°C) samples and their acid-treated products. In both sets, the acid reaction induces an increase in capacity with respect to the pristine oxide. However, the different structural and textural characteristics of each pristine solid lead to distinct electrochemical properties. In this way, sample B shows a continuous capacity fade for both acid treatments and the capacity values were significantly larger after acid treatment with the lower concentration of HNO_3. These results can be interpreted in terms of a less organized and rigid structure by comparison to the more crystalline C sample. Concentrated acid solution and subsequent cycling provoke structural distortion which affects capacity retention. In contrast, the deintercalated C samples showed lower capacity values and the sample obtained in 1 M HNO_3 for 24 h suffers a less marked capacity fade. These facts can be attributed to a higher structural rigidity of the more organized array of atoms in this oxide with a higher crystallinity even after acid treatment (Table 1).

Concerning electrochemical performance, it is noteworthy that the best capacities in the pristine samples were obtained for sample B (sample A showed particularly poor cycling behavior and thus was not included), probably as a compromise between composition and crystal perfection. For acid-treated samples, it is necessary to consider the effect of both proton exchange and crystallinity of the samples. This complicates the interpretation of the results. However, the larger initial capacities for both sets of acid-treated samples can be explained from the higher average oxidation

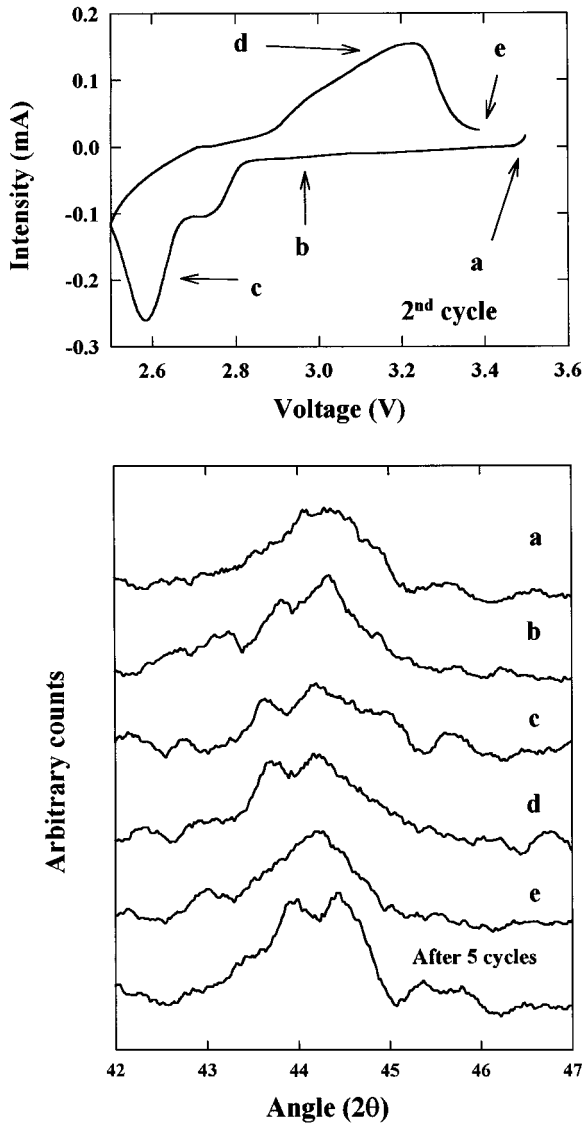

FIG. 6. X-Ray powder diffraction patterns in the region of (400) profiles obtained by interrupting SPES experiments of sample B after acid treatment with 0.1 M HNO_3 for 48 h at the points marked in the upper plot.

state of manganese. For the low-temperature samples, the larger amount of protons may undergo irreversible reactions with lithium, thus resulting in a more marked capacity fade. On the contrary, lower hydrogen content and higher crystallinity lead to better capacity retention in high-temperature samples.

To avoid electrolyte decomposition phenomena, the cycling behavior was tested in potentiostatic mode in a narrower potential window (2.5–3.5 V). For the study of electrochemical behavior under several kinetic conditions (Fig. 8), 0.1 N HNO_3 acid-treated samples were used. The narrower voltage range for lithiation (Fig. 8) results in an initially lower capacity but better capacity retention than in the wider interval (Fig. 7). As discussed above, higher capacity values are measured for the B samples. Moreover, the increase in rate has a stronger influence on C samples. This fact is probably due to the lower crystallite size of B samples which allows greater contact with the electrolyte and consequently better performance at higher rates. Nevertheless, it should be remarked that C samples have better capacity retention, particularly after the first cycle.

In conclusion, the use of nickel-containing $LiMn_2O_4$ combined with preliminary acid treatment improves cell capacity and cycling performance. Such improvements can be associated with changes in composition and crystallinity.

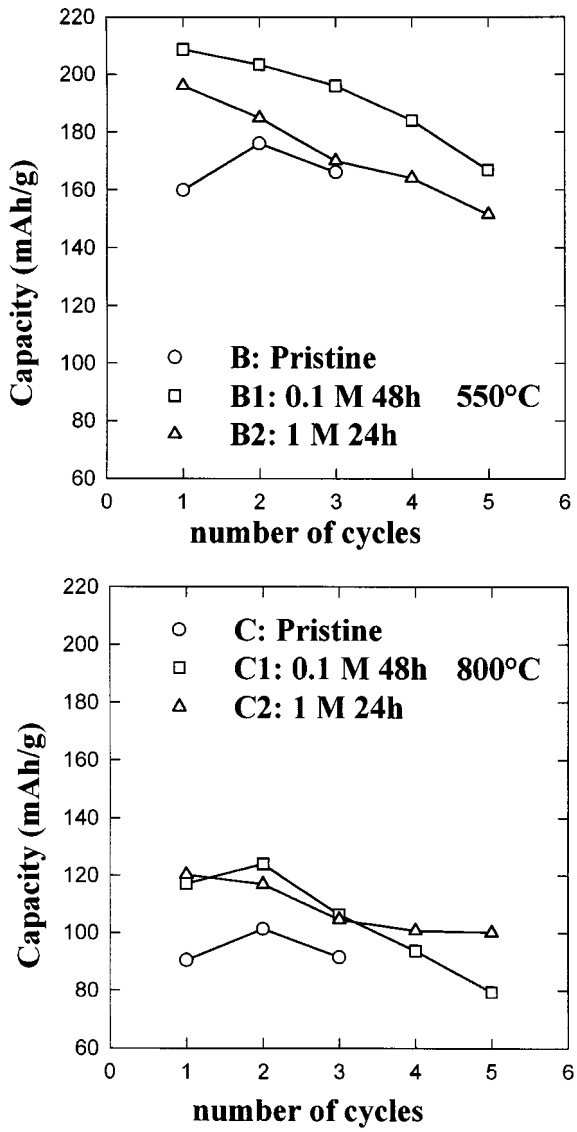

FIG. 7. Changes in cell capacity during the first few cycles in the potential window 2.0–4.4 V for pristine samples B (550°C) and C (800°C) and the products of acid treatment.

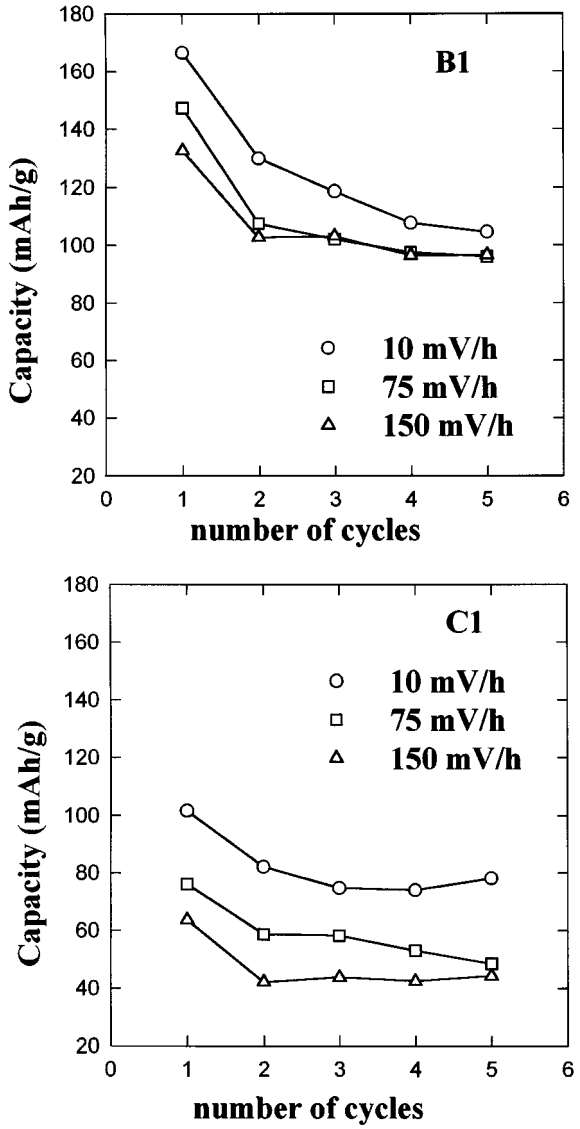

FIG. 8. Changes in cell capacity during the first few cycles for different rates in the potential window 2.5–3.5 V of B (550°C) and C (800°C) samples after acid treatment for 48 h with 0.1 M HNO_3.

An increase in the average oxidation state of manganese, a decrease in the Li/Mn ratio, and partial H^+/Li^+ exchange take place on acid treatment, simultaneously with a decrease in the unit cell parameters. As shown experimentally by X-ray diffraction line broadening analysis, the higher nickel contents and synthesis temperatures involve a slight improvement in crystallinity by acid treatment, while the opposite is true for samples below 800°C. The former effect is indicative of the dissolution of the external layers of the solid in which defects concentrate due to the proximity to the grain boundary while the latter reveals the distortions induced by a more extended H^+/Li^+ exchange. On the other hand, the electrode acid-treated solid releases lithium more easily during cell charge. For 800°C samples, the defective external layers behave as obstacles for lithium access to the electrolyte solution and crystallite size is reduced by dissolution. Finally, the role of nickel is of particular interest in stabilizing the spinel structure and allowing larger average oxidation states of manganese in the solid.

ACKNOWLEDGMENT

The authors acknowledge financial support from the French and Spanish governments through the PICASSO program (Contract HF 1997-0030).

REFERENCES

1. M. M. Thackeray, W. I. F. David, P. G. Bruce, and J. B. Goodenough, *Mater. Res. Bull.* **18,** 461 (1982).
2. M. H. Rossouw, A. De Kock, L. A. De Picciotto, and M. M. Thackeray, *Mater. Res. Bull.* **25,** 173 (1990).
3. J. M. Tarascon and D. Guyomard, *Electrochim. Acta* **38,** 1221 (1992).
4. D. H. Jang and S. M. Oh, *J. Electrochem. Soc.* **144,** 3342 (1997).
5. J. M. Tarascon, E. Wang, F. K. Schkoohi, W. R. Mckinnon, and S. Colson, *J. Electrochem. Soc.* **138,** 2859 (1991).
6. C. Sigala, D. Guyomard, A. Verbaere, Y. Piffard, and M. Tournoux, *Solid State Ionics* **81,** 167 (1995).
7. Q. Zhong, A. Bonakdarpour, M. Zhang, Y. Gao, and J. R. Dahn, *J. Electrochem. Soc.* **144,** 205 (1997).
8. B. J. Neudecker, R. A. Zuhr, J. D. Robertson, and J. B. Bates, *J. Electrochem. Soc.* **145,** 4160 (1998).
9. J. Morales, L. Sánchez, and J. L. Tirado, *J. Solid State Electrochem.* **2,** 420 (1998).
10. M. M. Thackeray, A. De Kock, M. H. Rossouw, D. Liles, R. Bittihn, and D. Hoge, *J. Electrochem. Soc.* **139,** 363 (1992).
11. L. Sánchez and J. L. Tirado, *J. Electrochem. Soc.* **144,** 1939 (1997).
12. R. J. Gummow and M. M. Thackeray, *J. Electrochem. Soc.* **140,** 3365 (1993).
13. R. Alcántara, J. Morales, J. L. Tirado, R. Stoyanova, and E. Zhecheva, *J. Electrochem. Soc.* **142,** 3997 (1995).
14. C. Pérez-Vicente, J. Morales, and J. L. Tirado, *Mater. Res. Bull.* **25,** 623 (1990).
15. J. C. Hunter, *J. Solid State Chem.* **39,** 142 (1981).
16. V. Manev, A. Momchilov, A. Nassalevska, and A. Sato, *J. Power Sources* **54,** 323 (1995).
17. D. Larcher, P. Courjal, R. Herrera Urbina, B. Gérand, A. Blyr, A. Du Pasquier, and J. M. Tarascon, *J. Electrochem. Soc.* **145,** 3392 (1998).
18. Q. Feng, Y. Miyai, H. Kanoch, and K. Ooi, *Langmuir* **8,** 1861 (1992).
19. Q. Feng, Y. Miyai, H. Kanoh, and K. Ooi, *Chem. Mater.* **5,** 311 (1993).
20. Q. Feng, H. Kanoh, Y. Miyai, and K. Ooi, *Chem. Mater.* **7,** 379 (1995).
21. R. A. Young and D. B. Wiles, *J. Appl. Crystallogr.* **15,** 430 (1982).
22. Y. Chabre, *J. Electrochem. Soc.* **138,** 329 (1991).
23. D. Wickham and W. Croft, *J. Phys. Chem. Solids* **7,** 351 (1958).
24. Y. F. Liu, Q. Feng, and K. Ooi, *J. Colloid Interface Sci.* **163,** 130 (1994).